Physics of Fluids

Computational analysis of hydrodynamic interactions in a high-density fish school

Cite as: Phys. Fluids **32**, 121901 (2020); https://doi.org/10.1063/5.0028682
Submitted: 06 September 2020 • Accepted: 17 November 2020 • Published Online: 04 December 2020

Yu Pan (潘宇) and Haibo Dong (董海波)

Physics of Fluids ARTICLE scitation.org/journal/phf

Computational analysis of hydrodynamic interactions in a high-density fish school

Cite as: Phys. Fluids 32, 121901 (2020); doi: 10.1063/5.0028682
Submitted: 6 September 2020 • Accepted: 17 November 2020 •
Published Online: 4 December 2020

Yu Pan (潘宇) and Haibo Dong (董海波)[a)]

AFFILIATIONS

Department of Mechanical and Aerospace Engineering, University of Virginia, Charlottesville, Virginia 22904, USA

[a)]Author to whom correspondence should be addressed: haibo.dong@virginia.edu

ABSTRACT

Numerical simulations are employed to study hydrodynamic interactions between two-dimensional fish-like bodies under a traveling wavy lateral motion in high-density diamond-shaped fish schools. This study focuses on two different streamwise spacings, a dense school with 0.4 body length (BL) spacing and a sparse school with 2.0 BL spacing, respectively. An immersed-boundary-method-based incompressible Navier–Strokes flow solver is then employed to quantitatively simulate the resulting flow patterns and associated propulsive performance of the schools. The results suggest that a fish in the dense school achieves higher thrust production and higher propulsive efficiency than that in the sparse school due to a strong wall effect from neighboring fishes. In addition, results from changing the lateral spacing in the dense school have shown that the wall effect is enhanced as the lateral spacing decreases. Flow analyses have shown that the wake pattern of the fish swimming diagonally behind the leading fish in a dense diamond-shaped school transfers from 2S to 2P when the lateral spacing is smaller than 0.6 BL. As a result, an angled jet is produced behind the school and brings more momentum downstream. At the same time, the appearance of the trailing fish results in a stronger pressure region behind the leading fish and leads to a higher hydrodynamic performance of the leading fish in the dense school. The insights revealed from this study will contribute to understanding physical mechanisms in fish schools and providing a new swimming strategy for bio-inspired underwater swarm robots.

I. INTRODUCTION

Fish schools, which are a typical naturally occurring form of aggregation, have been studied for decades. They are thought to provide several social advantages to fish,[1,2] including in predator avoidance,[3] in foraging,[4] and in reproduction.[5] Additionally, numerous experiments have provided evidence of hydrodynamic benefits for fish swimming in schools by showing a reduction in oxygen consumption and tail-beat frequency.[6,7] The spatial arrangement of the fish, which determines the density and shape of a school, is thought to be one of the most important factors influencing hydrodynamic interactions in the school swimming process.[8,9] Nevertheless, past research on the effect of the spatial arrangement on fish performance has been limited to sparse fish schools with a streamwise spacing of at least one body length (BL)[9,10] despite the fact that in nature, the snout of a fish is frequently ahead of the tail of the fish it is following.[2]

Experimental and computational studies on the effect of streamwise spacing[11–14] and lateral spacing[15–17] have been conducted for in-line configurations and side-by-side configurations, respectively. Boschitsch *et al.*[11] carried out an experimental study on two in-line pitching foils and suggested that for in-phase motion, the thrust production and propulsive efficiency of the downstream foil can be enhanced by 50% when the streamwise spacing is around a 1.2 chord length. By combining remeshed vortex methods and a deep reinforcement learning algorithm, Novati *et al.*[13] found that the "smart-follower" prefers to position itself 0.7 body length behind the leading fish, no matter where the initial position is, to achieve a 19.4% increase in average swimming efficiency. Dewey *et al.*[16] experimentally studied the performance of two oscillating foils in a side-by-side configuration and reported that when the lateral spacing is 0.5 chord length, the efficiency of the system can be enhanced by 35% with in-phase motion. This finding is consistent with that of the numerical study of Dong and Lu[15] on side-by-side undulating foils. Staggered formations have also received attention.[18–20] Li *et al.*,[18] using a three-dimensional overset-grid-based finite-volume method, built a full map of the hydrodynamic characteristics of fish swimming in pairs as functions of

the lateral spacing and streamwise spacing. They reported that the pair can save up to 3% of the cost of transport (COT) with in-phase motion in a staggered side-by-side formation. In an experimental study, Kurt *et al.*[19] reported that a following pitching foil can achieve a 63%–81% increase in thrust and efficiency when swimming in a staggered formation. All the aforementioned research demonstrates the significant effect of the spatial arrangement of the fish on the hydrodynamic interactions and energy efficiency of a fish school.

The performance of fish schools involving more than two fish has also been studied.[9,10,21,22] Using an analytical model, Weihs[8] studied a two-dimensional school of four fish constrained to a single plane. His findings suggested that a diamond configuration is the optimal formation for maximizing energy efficiency. Weihs[8] also proposed two possible mechanisms to explain the connection between the hydrodynamic interaction and the spatial arrangement of a school: the vortex hypothesis describes the constructive interaction between oncoming vortices and the following fish[8,23] and the channeling effect states that laterally neighboring fish swimming in close proximity can save energy by enhancing the flow between them.[8,10] However, the model was highly simplified and did not include the viscous effect of the flow. In recent years, using a multi-particle collision dynamics model, Hemelrijk *et al.*[9] numerically studied the hydrodynamic performance of various school configurations including diamond, rectangular, phalanx, and in-line patterns. Their results confirmed that a fish swimming in a diamond-configuration school can achieve higher efficiency than that undergoing solitary swimming but argued that the optimal lateral spacing is 1.6 BL rather than 0.4 BL suggested by Weihs.[8] In addition, Daghooghi and Borazjani[10] investigated the hydrodynamics of a mackerel school in rectangular configurations using three-dimensional flow simulations under periodic boundary conditions. It was found that the power efficiency of each fish swimming in a rectangular school increased by 8.8% when the lateral distance was 0.4 BL. Nevertheless, there is a lack of comprehensive investigation of the wake structures and associated hydrodynamic performance of dense fish schools, in which fishes are in close proximity to each other, using high-fidelity computational fluid dynamics flow simulations.

In this study, the vortex dynamics and hydrodynamic performance of dense schools in the diamond configuration are investigated using a high-fidelity immersed-boundary-method-based incompressible Navier–Stokes flow solver. In particular, the wall effect, resulting from the body–body interaction between lateral neighbors, is thoroughly investigated in dense schools by comparing the flow fields and hydrodynamic performance with those in sparse schools. Moreover, the block effect on vortex shedding from the leading fish, due to the close proximity of the trailing fish, in dense schools is also studied by simulating a triangular school. An outline of this paper is as follows. Section II describes the fish-like kinematics, the definition of a diamond school configuration, the numerical methods, the simulation setup, and the definition of performance parameters. The numerical results, including the hydrodynamic performance of a singular fish and that of different schools, are presented in Sec. III. The wall effect and the block effect in dense diamond-shaped schools are discussed in Sec. IV. Section V presents conclusions.

II. METHODS

A. Fish-like kinematics and school configuration

In this study, an NACA0012 foil is employed to represent a two-dimensional swimming body at an equilibrium state of undulating motion. To mimic fish-like swimming, traveling wave kinematics is imposed on the foil, similarly to the previous work.[15] For convenience, "fish" or "swimmers" are used to refer to foils in this paper. Considering that many sorts of carangiform fish have been reported to swim in schools,[24,25] we model the carangiform undulating motion in this work, and the traveling equation is

$$y(x,t) = A(x)\cdot\sin\left(\frac{2\pi}{\lambda}x - \frac{2\pi}{T}t\right), \tag{1}$$

where the position variables, x and y, are normalized by the body length L, so that $x = 0$ denotes the leading edge of a fish body and the trailing edge is at $x = 1$. The chord of the original foil is regarded as the fish spine, represented by $y = 0$ at rest, and $y(x, t)$ represents the lateral deviation for any point on the midline of the fish body at time t. λ denotes the wavelength of the traveling wave over an undulating body, and T is the wave period. $A(x)$ represents the amplitude envelope of a lateral motion and is expressed as a quadratic polynomial function,

$$A(x) = a_2x^2 + a_1x + a_0. \tag{2}$$

Based on the experimental data,[26] when the coefficients $a_0 = 0.02$, $a_1 = -0.08$, and $a_2 = 0.16$, the undulating motion can be defined as the carangiform motion. Figure 1 presents the amplitude envelope of a carangiform motion and a sequence of midlines during one tail-beat period.

Figure 2 shows the profiles of individual swimmers in a diamond-shaped school, where L is the body length and U_∞ is the swimming speed. The streamwise spacing S is defined as the distance between the tail of the leading fish (fish 1) and the head of the trailing fish (fish 4), and the lateral spacing D is defined as the spacing

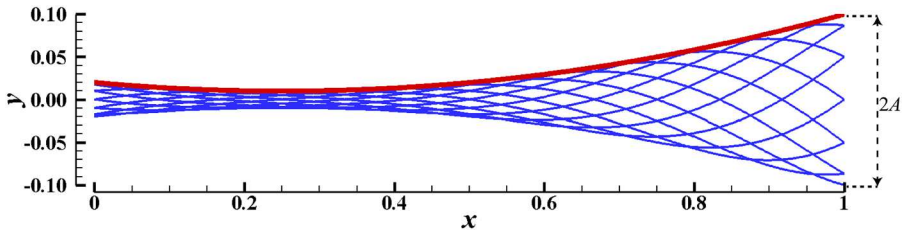

FIG. 1. Traveling wave amplitude of a carangiform motion (red line) and the motion of the fish-body midline during one tail-beat period (blue lines). A denotes the amplitude at the tail tip.

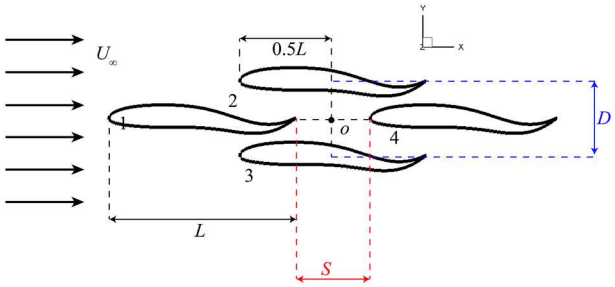

FIG. 2. Schematic of a diamond-shaped fish school and definitions of quantities describing its spatial arrangement.

between the centers of fish 2 and fish 3, which are on the lateral sides of the school. The whole school is symmetric in both the streamwise and lateral directions. For example, the distance between the tail of the leading fish and the black point o in Fig. 2 (the center of the school) is $S/2$, which is half the total streamwise spacing.

B. Numerical methods and case setup

In this study, the equations governing the flow are the two-dimensional continuity and incompressible viscous Navier–Stokes equations, which are written in the non-dimensional form as

$$\frac{\partial u_i}{\partial x_i} = 0, \quad \frac{\partial u_i}{\partial t} + \frac{\partial u_i u_j}{\partial x_j} = -\frac{1}{\rho}\frac{\partial p}{\partial x_i} + \nu\frac{\partial^2 u_i}{\partial x_i \partial x_j}, \tag{3}$$

where $i, j = 1, 2$ denote the x-direction and y-direction (repeated indices imply summation), u_i are the velocity components, p is the pressure, and ρ and ν denote the fluid density and the kinematic viscosity, respectively.

To solve the governing equations, an in-house immersed-boundary-based finite-difference flow solver is employed, which has been successfully applied to simulate biological fish swimming,[27] fish-like swimming,[28,29] and other forms of flapping propulsion.[30,31] More details about the method can be found in Ref. 32.

The computational domain and Cartesian computational grid used for simulating flow over traveling foils are presented in Fig. 3(a). In this study, fishes swim in the negative x-direction. The computational domain size is $20L \times 20L$, with 2337×897 grid nodes (about 2.10×10^6) in total. A high-resolution uniform grid is used in a region of size $6.0L \times 3.0L$ to solve the flow field near the swimmers. The minimum grid spacing is set as $\Delta_{min} = 3.50 \times 10^{-3}L$ in this study, which has been shown to be sufficiently fine at the relevant Reynolds number.[33] The left-hand boundary is the inflow boundary with a constant incoming flow velocity U_∞. At the right-hand boundary, the outflow boundary condition allows the vortices to move out of the domain without reflection. The upper and lower boundaries are set as zero-gradient boundaries with constant velocity U_∞ to represent free-stream conditions. A homogeneous Neumann boundary condition is applied for the pressure at all boundaries. In addition, a convergence study has been conducted to ensure that the results are grid-independent. Figure 3(b) presents the instantaneous net force coefficient in the x-direction for an isolated fish with three different grids. The minimum grid spacings of the coarse, medium, and fine meshes are $7.04 \times 10^{-3}L$, $3.50 \times 10^{-3}L$, and $2.04 \times 10^{-3}L$, respectively. This shows that the mean force difference between the medium grid case and the fine grid case is less than 1%, which demonstrates that the simulation results are grid-independent in this study.

In this work, two key parameters characterizing fish-like swimming, the Reynolds number Re and the Strouhal number St, are defined as follows:

$$Re = \frac{U_\infty L}{\nu}, \tag{4}$$

$$St = \frac{2fA}{U_\infty}, \tag{5}$$

where U_∞, L, and ν have the same meaning as stated above, f is the tail-beat frequency, and A is the amplitude of the lateral motion at the tail tip. We set the tail-beat frequency f as 1.0 and the amplitude at the tail tip A as 0.1 (shown in Fig. 1). The Reynolds number Re is set as 1000, a value relevant to fish swimming. In the present study, steady swimming is simulated for stable school formation by applying an incoming flow with constant velocity over fixed traveling wavy foils. The Strouhal number is thus obtained through Eq. (5) by changing the incoming flow speed U_∞ to meet the steady-swimming condition.

C. Definition of performance measures

The definitions of the hydrodynamic forces, power consumption, and propulsive efficiency are stated in the following. In our solver, the instantaneous forces are calculated by directly integrating the computed pressure and viscous stress on the surface of a fish

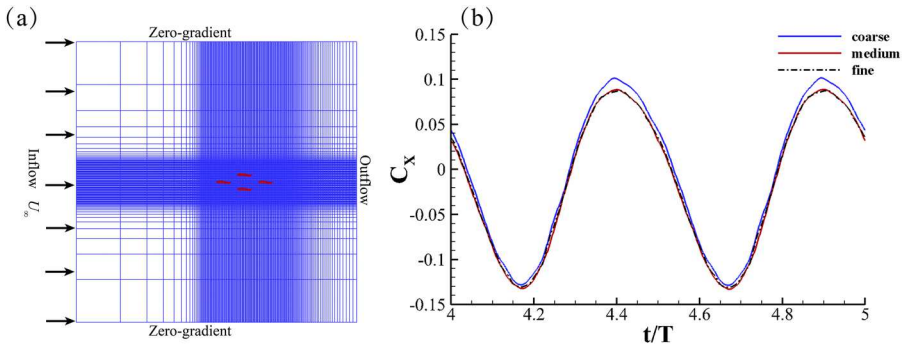

FIG. 3. (a) Schematic of the computational domain, Cartesian grids, and boundary conditions. (b) Comparison of the instantaneous net force coefficient in the x-direction of an isolated fish using coarse, medium, and fine meshes.

TABLE I. Strouhal numbers tested in this study.

Re	*A*	*f*	*L*	*St*
1000	0.1	1.0	1.0	0.3, 0.35, 0.4, 0.45, 0.5, 0.55, 0.6

and can be expressed as follows:

$$F_X = \int_S (-pn_x + \tau_{xi} n_i) dS, \tag{6}$$

$$F_Y = \int_S (-pn_y + \tau_{yi} n_i) dS, \tag{7}$$

where p is the pressure, the indices $i = 1, 2$ denote the x-direction and y-direction, respectively (repeated indices imply summation), n_i represents the i-th component of the unit normal vector on an element dS, and τ_{ij} is the viscous stress tensor.

In Eq. (6), F_X is the instantaneous net force in the x-direction on a fish body, which is the sum of the drag F_D and the thrust F_T calculated by the sign of the pressure and viscous stress acting on the surface[34] with respect to the swimming direction. In this paper, considering the coordinate system and the swimming direction, when $F_X < 0$, the fish produces a net thrust. Doing integral over the surface of the fish body, the thrust F_T can be computed as follows:

$$F_T = \frac{1}{2}\left(-\int_S -pn_x dS + \left|\int_S pn_x dS\right|\right) + \frac{1}{2}\left(-\int_S \tau_{xi} n_i dS + \left|\int_S \tau_{xi} n_i dS\right|\right). \tag{8}$$

The power required for the undulating motion can be defined as

$$P_u = \int_S (-pn_i + \tau_{ij} n_j) \Delta u_i dS, \tag{9}$$

where Δu_i is the velocity of an element dS relative to its surrounding fluid in the i-th direction. The forces and power, then, can be normalized by the swimming speed and the body length,

$$C_{X,Y} = \frac{F_{X,Y}}{\frac{1}{2}\rho U_\infty^2 L}, \; C_T = \frac{F_T}{\frac{1}{2}\rho U_\infty^2 L}, \; C_{PW} = \frac{P_u}{\frac{1}{2}\rho U_\infty^3 L}. \tag{10}$$

The definition of propulsion efficiency of undulating swimming is still controversial and varies depending on the assumptions and conditions utilized in different studies.[34–36] In this study, a modified form of Froude efficiency η is defined to measure the ratio of useful power to the total power,[37]

$$\eta = \frac{\overline{F_T} U_\infty}{\overline{F_T} U_\infty + \overline{P_u}} = \frac{\overline{C_T}}{\overline{C_T} + \overline{C_{PW}}}, \tag{11}$$

where the overline represents the time-averaged value during one tail-beat cycle. Here, the thrust $\overline{F_T}$ is used to calculate the propulsive efficiency on the swimming body, instead of the net force: as for steady swimming or quasi-steady swimming, the net-force-based propulsive efficiency is zero or close to zero, which results in the measurement of efficiency becoming too small and meaningless.[35]

III. RESULTS

A. Steady swimming of a single fish

To conveniently measure the hydrodynamic interactions, the initial condition is set as steady swimming; that is, the net force on each individual is zero at the beginning. The Reynolds number $Re = 1000$ is chosen for the following reasons: (1) the flow at this Reynolds number in two dimensions is similar to that at a much higher Re in three dimensions[9] and (2) this Reynolds number makes the viscous effect small enough but also able to contribute to maintaining a coherent vortex structure.[13] For a given Re, the time-averaged net force on a fish in the swimming direction is a function of the Strouhal number,[38] so the correct Strouhal number St can be obtained by measuring the net force on an isolated fish. The Strouhal number varies from 0.3 to 0.6, as shown in Table I. Figure 4(a) presents the time-averaged net force coefficient in the streamwise direction $\overline{C_X}$ for different Strouhal numbers. The shaded area below the dashed line denotes the increasing magnitude of the net thrust acting on the fish body. By interpolation, it is found that $St = 0.43$ satisfies the steady-swimming condition. It is also found that for a given Reynolds number, $\overline{C_X}$ decreases with the increasing Strouhal number from 0.3 to 0.6 [see Fig. 4(a)].

To elucidate the variation in hydrodynamic performance of an isolated fish at $St = 0.43$, we present the time histories of the net force

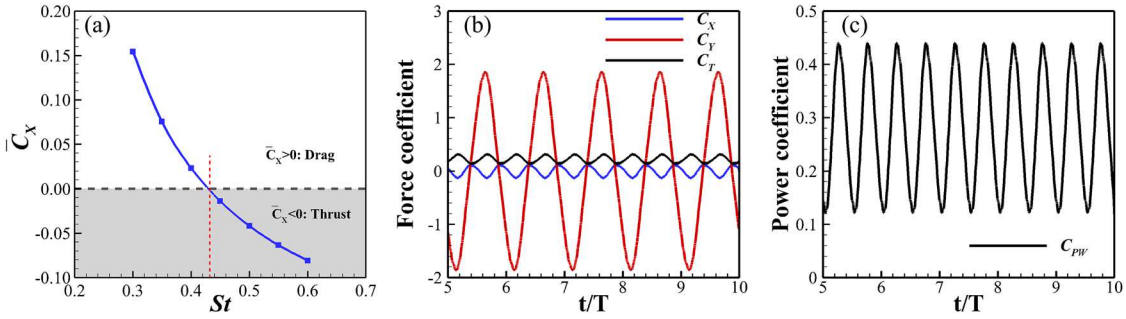

FIG. 4. (a) Time-averaged net force coefficient in the x-direction of an isolated fish at different St, where the shaded area below the dashed line denotes the increasing magnitude of the net thrust. Time histories of (b) the net force coefficient in the x-direction and y-direction and the thrust coefficient and (c) the undulating power coefficient at $St = 0.43$.

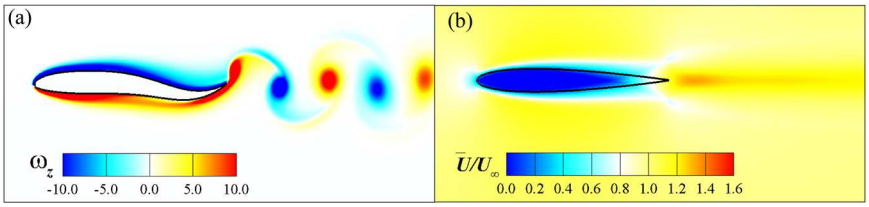

FIG. 5. (a) Vortex wake and (b) time-averaged streamwise velocity field of an isolated fish at $St = 0.43$.

coefficients in the x-direction and y-direction, the thrust coefficient, and the undulating power coefficient during five cycles in Figs. 4(b) and 4(c). The time-averaged net force coefficients can be obtained as $\overline{C_X} = -3.16 \times 10^{-4}$ and $\overline{C_Y} = -3.90 \times 10^{-4}$, which are close to zero, proving that the steady-swimming state has been reached. Figure 5 presents the vortex structure and the time-averaged streamwise velocity field of an isolated fish at $St = 0.43$. For the parameters considered in this work, the vortices shed by an undulating foil form a reverse von Kármán street [Fig. 5(a)].

B. Dense and sparse diamond-shaped schools

When the leading fish (fish 1) and the trailing fish (fish 4) are located in the channel formed by fish 2 and fish 3 in a diamond-shaped school (see Fig. 2), strong nonlinear body–body interactions between lateral neighbors occur, which have not yet been studied in depth. Two kinds of typical diamond-shaped schools, therefore, are designed here to study the body–body interactions in a fish school. In the dense school, the streamwise spacing S is equal to 0.4 BL, and fish 1 and fish 4 are located in the channel formed by fish 2 and fish 3. For comparison, the streamwise spacing is set as 2.0 BL in the sparse school, where fish 1 and fish 4 are both 0.5 BL away from the channel. The effect of the lateral spacing on the hydrodynamic performance in a diamond-shaped school is also studied.

Figure 6(a) presents the time-averaged net force in the x-direction $\overline{C_X}$ on each fish, and Fig. 6(b) shows the average value of $\overline{C_X}$ on the whole school. Due to symmetry and synchronization, fish 2 and fish 3 have the same hydrodynamic performance, so only the results for fish 2 are presented, while the average value for the whole system is computed from the performances of all four fishes.

As illustrated in Fig. 6(a), in the dense school, $\overline{C_X}$ for fish 1 changes from a net thrust to a net drag when the lateral spacing D goes above 0.65, while in the sparse school, $\overline{C_X}$ for fish 1 remains almost constant at around −0.025. In the dense school, fish 2 experiences a net thrust ($\overline{C_X} < 0$) when the lateral spacing $D < 0.6$, while a net drag ($\overline{C_X} > 0$) is applied to fish 2 in the sparse school when $D < 0.55$. In both schools, $\overline{C_X}$ for fish 2 tends to zero when the lateral spacing increases. In the dense school, $\overline{C_X}$ for fish 4 is much less than zero at around −0.09, and the absolute value decreases slowly with the increasing lateral distance. Fish 4 in the sparse school experiences a net thrust when $D < 0.45$ and $D > 0.8$, while it suffers a net drag when $0.45 \le D \le 0.8$. In Fig. 6(b), the average net force on the dense school is less than zero, and the absolute value decreases when the lateral spacing increases. In the sparse school, the average net force is a net drag when $0.4 < D \le 0.7$ and becomes a net thrust when $D > 0.7$.

Figure 7 shows the time-averaged thrust coefficient $\overline{C_T}$ for individuals in different schools as a function of the lateral spacing. It is found that in both the dense school and the sparse school, $\overline{C_T}$ for each fish, and the averaged value over the whole school, is higher than that of an isolated fish; that is, individuals in a school can always obtain a greater thrust production regardless of their position. In addition, as shown in Figs. 7(a) and 7(b), $\overline{C_T}$ values for individuals in the dense school ($S = 0.4$) monotonically rise with the decreasing lateral spacing, as opposed to those of individuals (except fish 4) in the sparse school, which only vary slightly. From Fig. 7(a), it is seen that when the lateral spacing is less than 0.65, $\overline{C_T}$ for fish 1 in the dense school is higher than that for fish 1 in the sparse school, while this is reversed when $D > 0.65$. When $D = 0.4$, the thrust on fish 1 in the dense school is 41.3% higher than that in the sparse

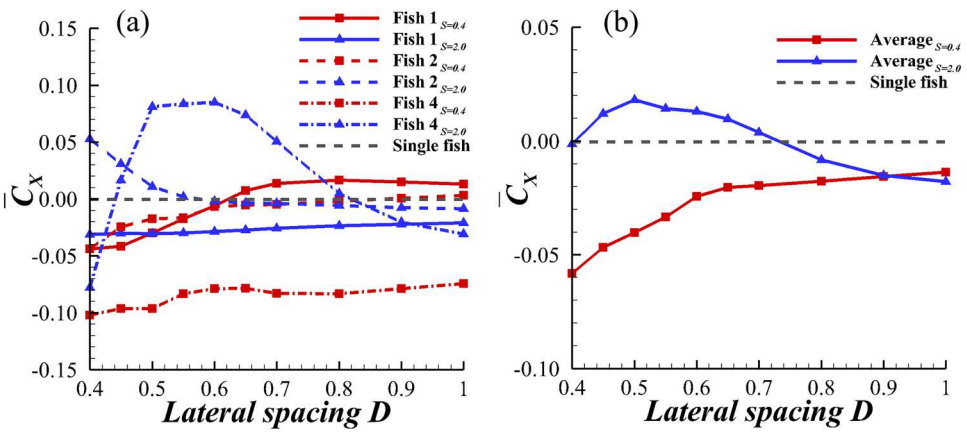

FIG. 6. Time-averaged net force in the x-direction on each fish as a function of the lateral spacing in the dense school ($S = 0.4$) and the sparse school ($S = 2.0$): (a) fish 1, fish 2, and fish 4; (b) the average net force on the whole school. The gray dashed line denotes the time-averaged net force on an isolated fish swimming steadily.

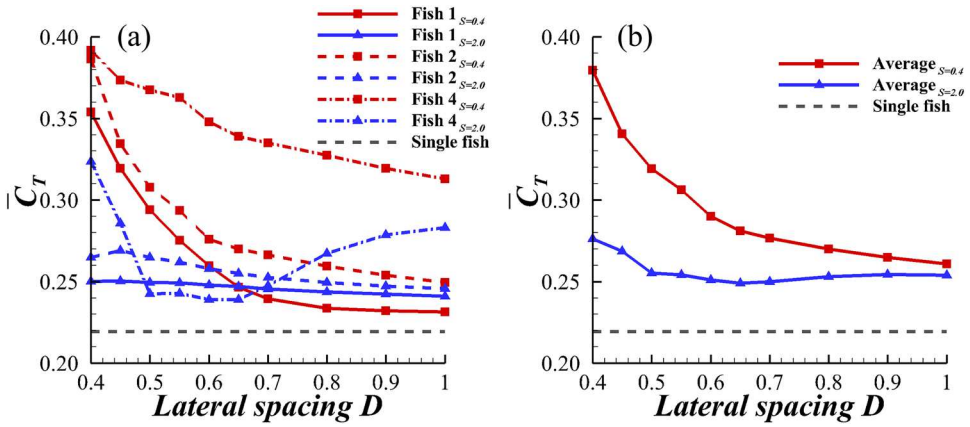

FIG. 7. Time-averaged thrust coefficient for each fish as a function of the lateral spacing in different schools (S = 0.4 and S = 2.0): (a) fish 1, fish 2, and fish 4; (b) the average thrust on the whole school. The gray dashed line denotes the time-averaged thrust coefficient of an isolated fish swimming steadily.

school. $\overline{C_T}$ for fish 1 increases by 53.2% in the dense school when the lateral spacing changes from 1.0 to 0.4, while in the sparse school, $\overline{C_T}$ for fish 1 remains at around 0.25 at all lateral spacings. Similar results are observed for fish 2, although here $\overline{C_T}$ is slightly larger than that for fish 1 at different lateral spacings in the dense school. $\overline{C_T}$ for fish 2 in the dense school increases by 56%, from 0.25 to 0.39, when the lateral spacing decreases from 1.0 to 0.4. As a comparison, the thrust on fish 2 in the sparse school shows a slight growth when the lateral spacing decreases [see Fig. 7(a)]. Furthermore, the difference in $\overline{C_T}$ for fish 2 between the dense school and the sparse school increases with the decreasing lateral spacing; when D = 0.4, $\overline{C_T}$ for fish 2 in the dense school is 45.8% higher than that in the sparse school.

In the dense school, even though $\overline{C_T}$ for fish 4 monotonically increases with the decreasing lateral spacing, the rate of increase is lower than that for fish 1 and fish 2 when $D < 0.7$. In the sparse school, however, $\overline{C_T}$ for fish 4 decreases with the increasing lateral spacing at lower values ($0.4 \le D < 0.5$), reaches a plateau from 0.5 to 0.65, and shows a concave rise with the increasing lateral spacing when $D \ge 0.65$ [see Fig. 7(a)]. Moreover, from Fig. 7(b), it is seen that the averaged $\overline{C_T}$ on the dense school rises monotonically, from 0.26 to 0.38, when the lateral spacing decreases from 1.0 to 0.4. Figure 7(b) also shows that the average thrust on the sparse school follows a similar variation to that on the dense school, although the rate of change and range of variation are much smaller. When D = 0.4, the average $\overline{C_T}$ on the dense school is 37.4% higher than that on the sparse school, and the difference in the average $\overline{C_T}$ between the two schools reaches its maximum value.

Figure 8 shows the propulsive efficiency η of each fish, and the average value of the whole school, in the two schools as a function of the lateral spacing. Here, for convenience, we use the first subscript to denote the school type and the second subscript to denote the fish; the dense school has subscript 1, and the sparse school has subscript 2. For example, the propulsive efficiency of fish 1 in the dense school is denoted η_{11}. First, it can be seen that η_{11} is lower than that of an isolated fish (η_{single} = 0.44), while η_{21} is higher than η_{single} and remains at around 0.47 when the lateral spacing changes from 0.4 to 1.0 [see Fig. 8(a)]. When $D < 0.6$, η_{11} increases with the increasing lateral spacing, and then, it decreases slowly from D = 0.6 to around 0.43 when $D \ge 0.7$. Second, η_{12} increases by 18.8%, from 0.48 to 0.57, when the lateral spacing decreases from 1.0 to 0.4, while η_{22} remains at around 0.47. Third, the propulsive efficiencies of fish 4 show opposite trends in the dense school and in the sparse school [see Fig. 8(a)]. When $D < 0.55$, η_{14} rises, but η_{24} falls with the increasing lateral

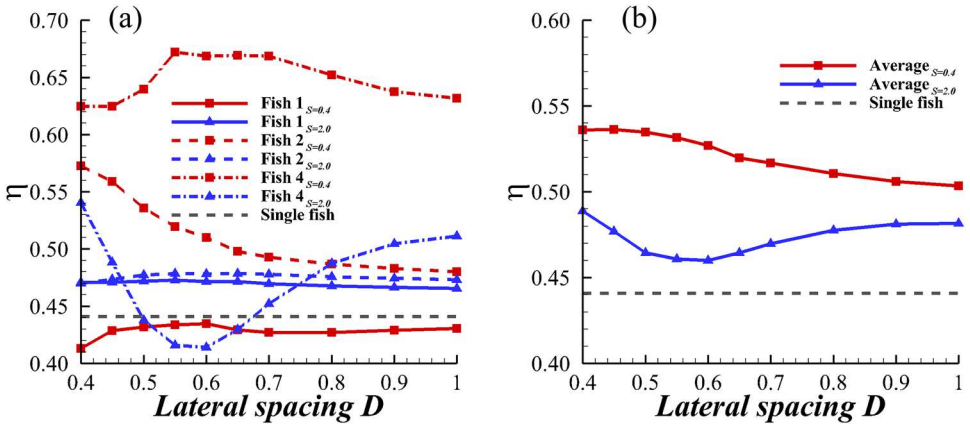

FIG. 8. Propulsive efficiency of each fish as a function of the lateral spacing in different schools (S = 0.4 and S = 2.0): (a) fish 1, fish 2, and fish 4; (b) the average propulsive efficiency of the whole school. The gray dashed line denotes the time-averaged propulsive efficiency of an isolated fish swimming steadily.

spacing. When D = 0.55, η_{14} reaches its maximum value η_{14_max} = 0.67 and η_{24} reaches its minimum value η_{24_min} = 0.42. When D increases further, both η_{14} and η_{24} reach a plateau where the propulsive efficiencies remain almost unchanged. Then, η_{14} decreases when $D > 0.7$, and η_{24} rises when $D > 0.6$. In the sparse school, due to the wider streamwise spacing, fish 4 is barely influenced by the body–body interaction imposed by its lateral neighbors but mainly affected by the vortex wake shed by the fish in front. Thus, the opposite trends suggest that when involving the body–body interactions, the vortex wake can impose an opposing effect on the propulsive efficiency. Finally, the average propulsive efficiency of the dense school is at least 4.5% higher than that of the sparse school, and they are both higher than η_{single} [see Fig. 8(b)]. The average propulsive efficiency of the dense school η_{1a} increases by 8.0%, from 0.50 to 0.54, when the lateral spacing decreases from 1.0 to 0.4, while η_{2a} shows a similar trend to η_{24} but within a smaller range.

From Figs. 6(a), 7(a), and 8(a), it is seen that compared with those for the other fish, C_X, C_T, and η for fish 4 vary in a more complicated way in both the dense school and the sparse school. Being located at the rear of the school, fish 4 occupies a more chaotic flow environment and is influenced by various hydrodynamic interactions, including the lateral body–body interaction and the vortex wake interaction that will be explored in further research.

IV. DISCUSSION

A. Wall effect in a dense school

From Figs. 7(a) and 8(a), it is seen that the hydrodynamic performance of fish 2 in the dense school is much better than that in the sparse school, and the difference increases with the decreasing lateral spacing. In particular, when D = 1.0, $\overline{C_T}$ and η for fish 2 in the dense school are both 1.5% higher than those in the sparse school; when D = 0.4, $\overline{C_T}$ for fish 2 in the dense school is 37.4% higher, and η is 21.9% higher. This significant improvement in hydrodynamic performance suggests that there is a strong hydrodynamic effect acting on fish 2 in the dense school.

An experimental study by Quinn *et al.*[39] found that for an oscillating foil near a solid boundary, the thrust can be enhanced by 40% consuming little extra power when the foil is 0.4 chord length from the ground. Quinn *et al.*[40] also reported that a flexible propulsor can obtain hydrodynamic benefits when swimming near the ground. In the previous research,[15] it has been shown that for an isolated undulating foil, the thrust is mainly produced at the tail. Thus, based on our results and those of previous studies, we assume that in a dense diamond-shaped school, when fish 2 is close to fish 4 in the lateral direction, the body of fish 4 acts like a wavy wall to fish 2 (see Fig. 2). The wall effect is, therefore, applied to the body–body interaction produced by lateral neighbors in a dense school and investigated in this subsection by analyzing flow fields.

It is found that the time-averaged thrust coefficient and propulsive efficiency of fish 2 in the dense school monotonically increase with the decreasing lateral spacing D. In particular, when the lateral spacing reduces from 0.6 to 0.4, $\overline{C_T}$ for fish 2 in the dense school increases by 39%, from 0.28 to 0.39, and the propulsive efficiency η increases by 12%, from 0.51 to 0.57. They vary slowly when $D > 0.6$ [see Figs. 7(a) and 8(a)]. A comparison indicates that the wall effect on fish 2 in the dense school weakens with the increasing lateral spacing. Thus, according to the behavior at different lateral spacings, the wall effect can be divided into two regimes: $0.4 \le D \le 0.6$ and $D > 0.6$. We identify a typical dense school in each regime: school A (D = 0.4, S = 0.4) and school B (D = 1.0, S = 0.4), and compare and analyze their flow characteristics.

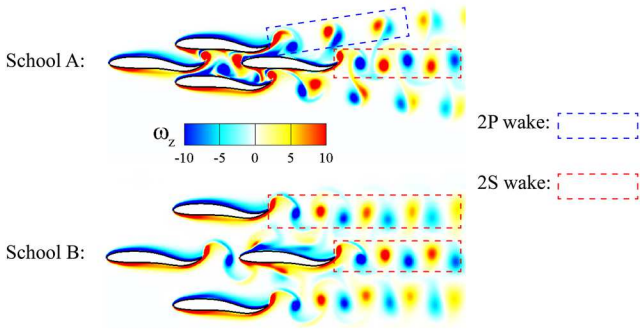

FIG. 9. Vortex wake of school A (top, D = 0.4, S = 0.4) and school B (bottom, D = 1.0, S = 0.4) at $t = 10T$. A 2P wake is marked by a blue dashed square, and a 2S wake is marked by a red dashed square.

Figure 9 shows the vortex fields of school A and school B at $t = 10T$. Vortices shed by an isolated undulating foil form an archetypal reverse von Kármán street (2S wake) for the parameters considered in the present study [see Fig. 5(a)], which can also be found in the wakes of school A and school B (see Fig. 9). However, owing to the close proximity in the lateral direction, the stability has been broken, and vortex pairs are formed in the wake of school A, as shown in Fig. 9. A similar pairing was reported by Quinn *et al.*[39] when they studied a rigid pitching foil near the ground. By checking the vortex wake of all dense schools in this study, we find that the vortex wake of fish 2 and fish 3 transfers from 2S to 2P when $D \le 0.6$, that

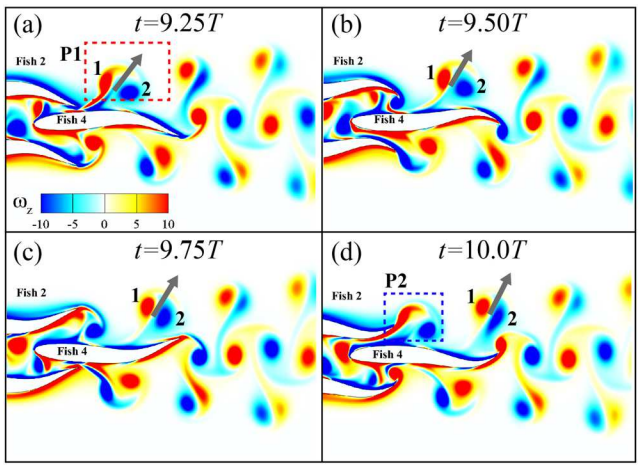

FIG. 10. Process of vortex pairing and advection during the tenth cycle (a)–(d). The gray arrows denote the direction of a vortex pair. The positive vortex (red) is denoted vortex 1, and the negative vortex (blue) is vortex 2. P1 is the first vortex pair shed by fish 2, marked by a red dashed square in (a), and P2 is the second vortex pair, marked by a blue dashed square in (d).

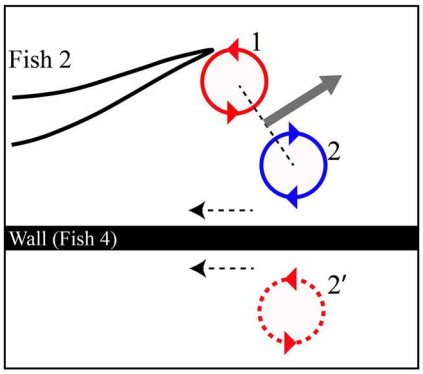

FIG. 11. Use of the method of images and vortex induction theory to explain the formation of a vortex pair. The gray arrow denotes the direction of the vortex pair, and the dashed circle denotes the opposite-sign image vortex. The dashed arrows denote the direction of induced velocity.

is, the spatial arrangement can significantly change the wake pattern of a school. In addition, Fig. 9 shows that vortices shed by fish 2 in school A are stronger than those in school B, which means that the shedding vortices of fish 2 are enhanced when the lateral spacing is small.

Two distinct phenomena relating to the vortex wake of school A are identified during the pairing process [see Figs. 10(a)–10(d)]. In this study, we define the direction of a vortex pair as perpendicular to the line connecting the cores of two vortices and parallel to the advection direction, which is denoted by gray arrows in Fig. 10. Initially, from Figs. 10(a)–10(d), it is seen that the angle between the direction of a vortex pair shed by fish 2 and the flow direction gradually increases while the pair advects downstream. Then, Fig. 10 shows that the negative (blue) vortex decays faster than the positive (red) vortex in a vortex pair and the negative vortex has been stretched during advection [see vortex 2 in Figs. 10(c) and 10(d)]. The method of images[39] and vortex induction theory can be applied to explain these phenomena. Figure 11 illustrates the formation of a vortex pair using the method of images. For each vortex shed by fish 2, there is an opposite-sign image vortex beneath the boundary (the top surface of fish 4) to satisfy the no-flux boundary condition. According to the Biot–Savart law, vortex 2 (negative) is slowed by the opposite-sign image (vortex 2′), while vortex 1 speeds up due to the induction from its image vortex. Then, a vortex pair is formed because of the advection-velocity difference between vortex 1 and vortex 2. The mutual induction between vortex 1 and vortex 2 also contributes to the formation of the vortex pair. However, this mutual induction only occurs after the pairing process initiates and is thus assumed to take a secondary role. Thereafter, the mutual induction leads the vortex pair to move away from the boundary while advecting downstream.

The negative vortex shed by fish 2 is stretched when moving downstream due to the mutual induction with the boundary-layer vortex of fish 4, shown by the variation of vortex 2 in Figs. 10(c) and 10(d). The boundary-layer vortex can also slow the motion of vortex 2 by induction. Furthermore, stretching results in a decay of vortex 2, as shown in Figs. 10(d) and 12. The strength of vortex 2 thus gradually reduces, while vortex 1 almost maintains its vortex strength while advecting downstream. The discrepancy in strength causes the vortex pair to rotate in an anticlockwise direction, shown in Fig. 12(b), which results in the advection direction of the vortex pair moving closer to the vertical. While fish 3 follows a similar behavior to fish 2 because of symmetry, the signs of its shedding vortices are opposite.

The motion of the vortices delivers momentum downstream, and locomotive forces are produced. Figure 13 displays the time-averaged streamwise velocity field of school A and school B. An angled high-density velocity jet has formed behind fish 2 and fish 3 in school A, which is expected when angled shedding vortices of fish 2 move downstream (see Fig. 10). The stronger jet indicates that more streamwise momentum[41] has been transported downstream. Fish 2 in school A, therefore, has a higher thrust production.

B. Block effect in a dense school

In a finite fish school, a fish can experience the wall effect, as fish 2 does in a dense diamond-shaped school. In an infinite school, however, many fish may be located in the channel formed by laterally neighboring fish in a staggered manner, like the leading fish (fish 1) in the dense school. The channeling effect is quite different from the wall effect described in Sec. IV A. Besides, in a dense diamond-shaped school, fish 1 is also influenced by fish 4. Further research on the hydrodynamic performance of fish 1 in a dense diamond-shaped school is, therefore, needed.

Owing to the wall effect, fish 2 in a dense school has a higher thrust production and a higher propulsive efficiency than that in a sparse school. On the other hand, it is found that fish 1 in a dense

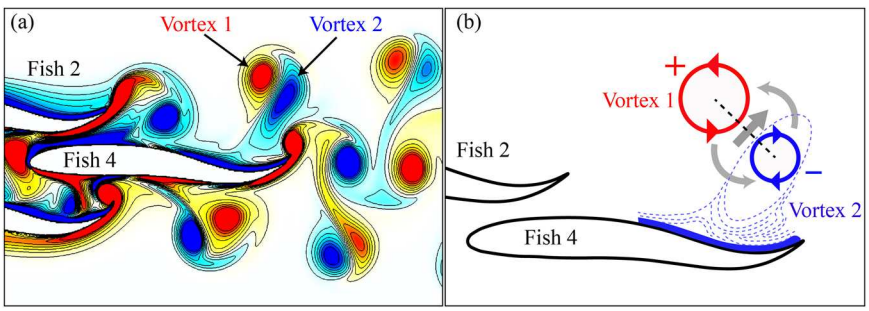

FIG. 12. The mutual induction and the stretching of vortices illustrate the decay of the negative vortex (vortex 2) in a vortex pair and the rotation of the vortex pair. (a) A vortex pair composed of vortex 1 and vortex 2 in the vorticity field; (b) a schematic of vortex stretching and vortex-pair rotation. The straight gray arrow denotes the direction of the vortex pair, and the curved gray arrows denote the rotating direction of the vortex pair.

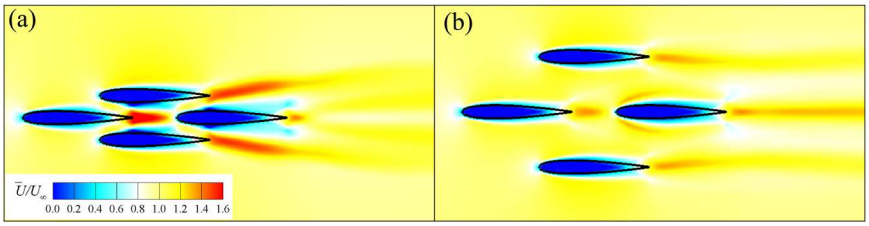

FIG. 13. Time-averaged streamwise velocity field of (a) school A and (b) school B.

school has a higher thrust [Fig. 7(a)] but a lower propulsive efficiency [Fig. 8(a)]. These differences in the variation of propulsive efficiency of fish 1 and fish 2 represent one of the differences between the channeling effect and the wall effect. It can be shown that while the thrust of fish 1 in the dense school increases with the decreasing lateral distance, the lateral force substantially increases, meaning more power is consumed to produce the lateral undulating motion. The propulsive efficiency can, therefore, be even lower than that of a single fish [Fig. 8(a)]. Considering the higher efficiency of the other members, this implies that the leading fish sacrifices its propulsive efficiency to benefit other members in a dense school. The above analysis also makes clear that it may not be sufficient to only consider the effect of neighboring swimmers preventing the wake of a swimmer freely expanding in the lateral direction, to illustrate the hydrodynamic benefits of the channeling effect in a fish school.

What, then, is the role of fish 4 in the hydrodynamic performance of fish 1 in a dense school? To answer this question, we compare the hydrodynamic performance of a dense diamond-shaped school ($S = 0.4$) and the corresponding triangular school in which fish 1, fish 2, and fish 3 are located in the same positions as in the diamond-shaped school.

Figure 14 shows the time-averaged thrust coefficient and propulsive efficiency of fish 1 as a function of the lateral spacing in dense diamond-shaped and triangular schools. In Fig. 14(a), with the decreasing lateral spacing, the thrust coefficient rises, both in the diamond-shaped school and in the triangular school. $\overline{C_T}$ for fish 1 in the diamond-shaped school is at least 17.8% higher than that for fish 1 in the triangular school, and the difference in thrust production between the two schools increases with the decreasing lateral spacing [see Fig. 14(a)]. In addition, when $D > 0.55$, $\overline{C_T}$ for fish 1 in a triangular school is even less than that for an isolated fish. In Fig. 14(b), the propulsive efficiency of fish 1 in both schools is lower than that of an isolated fish. However, it is found that the propulsive efficiency of fish 1 in the diamond-shaped school is at least 17.8% higher than that of fish 1 in the triangular school. In short, fish 1 in the dense diamond-shaped school has a higher thrust production and a higher propulsive efficiency than that in the triangular school.

Sometimes, destructive hydrodynamic interactions are unavoidable for certain fish in a school. For example, fish 1 needs to consume more energy as a sacrifice for other members in a dense school, as stated above. However, the results suggest that the loss of the propulsive efficiency of fish 1 can be reduced by placing fish 4 at the rear of the channel formed by fish 2 and fish 3. Flow comparisons between a diamond-shaped school and a triangular school provide insight into how fish 1 obtains a better hydrodynamic performance in a dense diamond-shaped school. Figure 15 presents the vorticity fields at $t = 10.0T$, the time-averaged streamwise velocity fields, and the time-averaged pressure fields of a dense diamond-shaped school ($D = 0.4$, $S = 0.4$) and the corresponding triangular school.

From Fig. 15, it is seen that the flow fields of the triangular school are quite different from those of the diamond-shaped school. Behind the triangular school, the vortex wake in the middle is weaker and more chaotic [Fig. 15(a)], which is due to the vortices shed by fish 1 interacting with the vortices shed by fish 2 and fish 3, separately. Negative vortices are left behind fish 2, and positive vortices behind fish 3, and both are both arranged on a line when advecting downstream, instead of generating 2S or 2P wakes. In comparison,

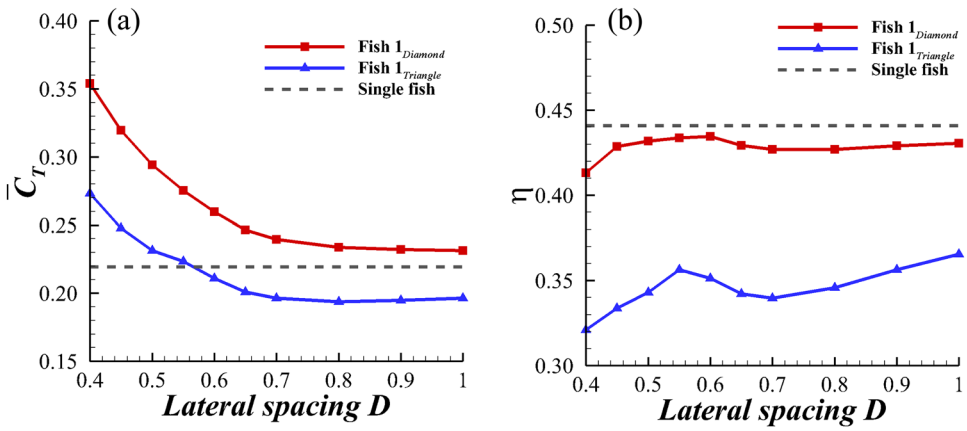

FIG. 14. Time-averaged thrust coefficient (a) and propulsive efficiency (b) of fish 1 as a function of the lateral spacing in dense diamond-shaped schools ($S = 0.4$) and triangular schools. The gray dashed line denotes the corresponding values for an isolated fish swimming steadily.

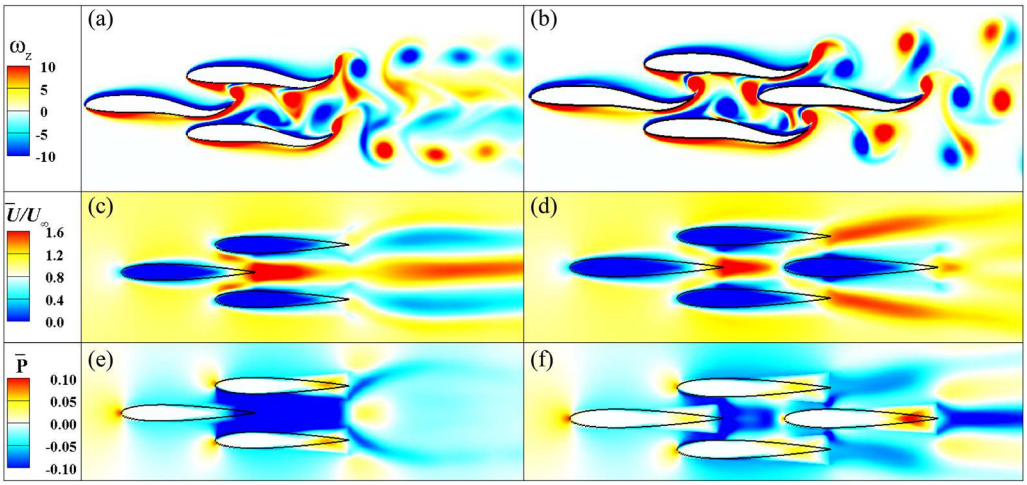

FIG. 15. Vorticity fields [(a) and (b)] at $t = 10.0T$, time-averaged streamwise velocity fields [(c) and (d)], and time-averaged pressure fields [(e) and (f)] over one tail-beat period of a triangular school [(a), (c), and (e)] and a diamond-shaped school ($D = 0.4$, $S = 0.4$) [(b), (d), and (f)].

in the diamond-shaped school, the presence of fish 4 impedes the interactions between the vortex wakes of fish 1 and fish 2, and an angled 2P wake is generated behind fish 2; this also happens to fish 3. Correspondingly, a straight jet is produced behind the triangular school, while two separate angled jets are produced behind the diamond-shaped school. Moreover, there are two small jets in front of the tail of fish 1 in the triangular school [see Fig. 15(c)], indicating that some momentum has been transported upstream, which is detrimental to the efficiency of the system.

Because fish 4 prevents the interactions between the vortex wakes and redirects the flow in the channel formed by fish 2 and fish 3, the pressure around the tail of fish 1 in the diamond-shaped school is much higher than that in the triangular school [see Figs. 15(e) and 15(f)]. Therefore, considering that the thrust is mainly produced at the tail of a fish and that pressure is the dominant part of the thrust, the different pressure fields mean that fish 1 produces a higher thrust in the diamond-shaped school than in the triangular school. Moreover, the pressure behind fish 1 is higher in the diamond-shaped school, while the pressure distributions in front of fish 1 in the two schools are almost the same. It can, therefore, be derived that fish 1 in the triangular school has a higher form drag than that in the diamond-shaped school, which illustrates that the difference in net force ($\Delta\overline{C_X} = 0.20$) on fish 1 between the two schools is higher than the difference in thrust ($\Delta\overline{C_T} = 0.08$). It is thus safe to conclude that the presence of fish 4, which works like a block preventing the interaction between the vortex wakes and enhancing the pressure field between fish 1 and fish 4 in the channel, essentially improves the thrust production and the propulsive efficiency of fish 1 in a dense diamond-shaped school. It appears that fish 1 is propelled by fish 4 in a dense diamond-shaped school, and we call this effect the block effect.

V. CONCLUSION

In this work, an immersed-boundary-method-based flow solver is employed to investigate the effects of the spatial arrangement of the fish on the hydrodynamic performance and wake structures of a diamond-shaped fish school in low Reynolds number ($Re = 1000$) flows. First, the results suggest that in a dense school, in which the streamwise spacing is 0.4 BL, the thrust production and the propulsive efficiency of the lateral fishes that are diagonally located in the school are substantially enhanced due to a wall effect imposed by the trailing fish. This wall effect is enhanced when the lateral spacing decreases. Flow analysis shows that when the lateral spacing is less than 0.6 BL, the vortices shed by the lateral fish start pairing and the wake expands in the lateral direction. Correspondingly, an angled jet is generated behind the lateral fish, which results in a high thrust production by the fish. This change in the wake patterns has commonly been ignored in past analytical models used for studying dense fish schools.

Second, in dense schools, the block effect imposed by the trailing fish on the performance of the leading fish is substantial. When the lateral spacing reaches 0.4 BL, the thrust produced by the leading fish in the diamond-shaped school is 29.6% higher than that in a triangular school without the trailing fish, and its hydrodynamic efficiency is 28.7% higher. Wake analysis reveals that in a dense diamond-shaped school, the trailing fish redirects the flow in the channel formed by the lateral fish and prevents interactions between the wakes shed by the leading fish and the lateral fish. This creates a stable high-pressure zone between the leading fish and the trailing fish in the channel and consequently enhances the thrust production of the leading fish. These findings provide new insight into the channeling effect and reveal the positive influence of the trailing fish on the performance of the leading fish in dense schools.

SUPPLEMENTARY MATERIAL

The supplementary material presents two videos of different vortex wakes in Fig. 9.

ACKNOWLEDGMENTS

This work was supported under Grant Nos. ONR MURI N0014-14-1-0533 and NSF CNS-1931929.

DATA AVAILABILITY

The data that support the findings of this study are available from the corresponding author upon reasonable request.

REFERENCES

[1]E. Shaw, "Schooling fishes: The school, a truly egalitarian form of organization in which all members of the group are alike in influence, offers substantial benefits to its participants," Am. Sci. **66**, 166 (1978); available at https://www.jstor.org/stable/27848512

[2]B. L. Partridge, "The structure and function of fish schools," Sci. Am. **246**, 114 (1982).

[3]V. E. Brock and R. H. Riffenburgh, "Fish schooling: A possible factor in reducing predation," ICES J. Mar. Sci. **25**, 307 (1960).

[4]T. J. Pitcher, *Functions of Shoaling Behaviour in Teleosts* (Springer, 1986).

[5]J. J. Cech and P. B. Moyle, *Fishes: An Introduction to Ichthyology* (Pearson/B. Cummings, 2004).

[6]J. Herskin and J. F. Steffensen, "Energy savings in sea bass swimming in a school: Measurements of tail beat frequency and oxygen consumption at different swimming speeds," J. Fish Biol. **53**, 366 (1998).

[7]S. S. Killen, S. Marras, J. F. Steffensen, and D. J. McKenzie, "Aerobic capacity influences the spatial position of individuals within fish schools," Proc. R. Soc. B **279**, 357 (2012).

[8]D. Weihs, "Hydromechanics of fish schooling," Nature **241**, 290 (1973).

[9]C. K. Hemelrijk, D. A. P. Reid, H. Hildenbrandt, and J. T. Padding, "The increased efficiency of fish swimming in a school," Fish Fish. **16**, 511 (2015).

[10]M. Daghooghi and I. Borazjani, "The hydrodynamic advantages of synchronized swimming in a rectangular pattern," Bioinspiration Biomimetics **10**, 056018 (2015).

[11]B. M. Boschitsch, P. A. Dewey, and A. J. Smits, "Propulsive performance of unsteady tandem hydrofoils in an in-line configuration," Phys. Fluids **26**, 051901 (2014).

[12]I. Akhtar, R. Mittal, G. V. Lauder, and E. Drucker, "Hydrodynamics of a biologically inspired tandem flapping foil configuration," Theor. Comput. Fluid Dyn. **21**, 155 (2007).

[13]G. Novati, S. Verma, D. Alexeev, D. Rossinelli, W. M. van Rees, and P. Koumoutsakos, "Synchronisation through learning for two self-propelled swimmers," Bioinspiration Biomimetics **12**, 036001 (2017).

[14]G. D. Xu, W. Y. Duan, and W. H. Xu, "The propulsion of two flapping foils with tandem configuration and vortex interactions," Phys. Fluids **29**, 097102 (2017).

[15]G.-J. Dong and X.-Y. Lu, "Characteristics of flow over traveling wavy foils in a side-by-side arrangement," Phys. Fluids **19**, 057107 (2007).

[16]P. A. Dewey, D. B. Quinn, B. M. Boschitsch, and A. J. Smits, "Propulsive performance of unsteady tandem hydrofoils in a side-by-side configuration," Phys. Fluids **26**, 041903 (2014).

[17]Y. Bao, D. Zhou, J. J. Tao, Z. Peng, H. B. Zhu, Z. L. Sun, and H. L. Tong, "Dynamic interference of two anti-phase flapping foils in side-by-side arrangement in an incompressible flow," Phys. Fluids **29**, 033601 (2017).

[18]G. Li, D. Kolomenskiy, H. Liu, B. Thiria, and R. Godoy-Diana, "On the energetics and stability of a minimal fish school," PLoS One **14**, e0215265 (2019).

[19]M. Kurt, A. Eslam Panah, and K. W. Moored, "Flow interactions between low aspect ratio hydrofoils in in-line and staggered arrangements," Biomimetics **5**, 13 (2020).

[20]Z.-R. Peng, H. Huang, and X.-Y. Lu, "Collective locomotion of two self-propelled flapping plates with different propulsive capacities," Phys. Fluids **30**, 111901 (2018).

[21]D. Jian and X.-m. Shao, "Hydrodynamics in a diamond-shaped fish school," J. Hydrodyn., Ser. B **18**, 438 (2006).

[22]S.-Y. Chen, Y.-H. J. Fei, Y.-C. Chen, K.-J. Chi, and J.-T. Yang, "The swimming patterns and energy-saving mechanism revealed from three fish in a school," Ocean Eng. **122**, 22 (2016).

[23]J. C. Liao, "A review of fish swimming mechanics and behaviour in altered flows," Philos. Trans. R. Soc., B **362**, 1973 (2007).

[24]L. P. Hansen and B. J. A. Jonsson, "Downstream migration of hatchery-reared smolts of Atlantic salmon (Salmo salar L.) in the River Imsa, Norway," Aquaculture **45**, 237 (1985).

[25]B. L. Partridge, J. Johansson, and J. Kalish, "The structure of schools of giant bluefin tuna in Cape Cod Bay," Environ. Biol. Fishes **9**, 253 (1983).

[26]J. Videler and F. Hess, "Fast continuous swimming of two pelagic predators, saithe (*Pollachius virens*) and mackerel (*Scomber scombrus*): A kinematic analysis," J. Exp. Biol. **109**, 209 (1984); available at https://jeb.biologists.org/content/109/1/209.short

[27]G. Liu, Y. Ren, H. Dong, O. Akanyeti, J. C. Liao, and G. V. Lauder, "Computational analysis of vortex dynamics and performance enhancement due to body-fin and fin-fin interactions in fish-like locomotion," J. Fluid Mech. **829**, 65 (2017).

[28]P. Han, G. V. Lauder, and H. Dong, "Hydrodynamics of median-fin interactions in fish-like locomotion: Effects of fin shape and movement," Phys. Fluids **32**, 011902 (2020).

[29]M. S. U. Khalid, J. Wang, H. Dong, and M. Liu, "Flow transitions and mapping for undulating swimmers," Phys. Rev. Fluids **5**, 063104 (2020).

[30]C. Li and H. Dong, "Three-dimensional wake topology and propulsive performance of low-aspect-ratio pitching-rolling plates," Phys. Fluids **28**, 071901 (2016).

[31]H. Dong, Z. Liang, and M. Harff, "Optimal settings of aerodynamic performance parameters in hovering flight," Int. J. Micro Air Veh. **1**, 173 (2009).

[32]R. Mittal, H. Dong, M. Bozkurttas, F. M. Najjar, A. Vargas, and A. von Loebbecke, "A versatile sharp interface immersed boundary method for incompressible flows with complex boundaries," J. Comput. Phys. **227**, 4825 (2008).

[33]M. S. U. Khalid, I. Akhtar, and H. Dong, "Hydrodynamics of a tandem fish school with asynchronous undulation of individuals," J. Fluids Struct. **66**, 19 (2016).

[34]I. Borazjani and F. Sotiropoulos, "Numerical investigation of the hydrodynamics of carangiform swimming in the transitional and inertial flow regimes," J. Exp. Biol. **211**, 1541 (2008).

[35]A. P. Maertens, M. S. Triantafyllou, and D. K. P. Yue, "Efficiency of fish propulsion," Bioinspiration Biomimetics **10**, 046013 (2015).

[36]W. W. Schultz and P. W. Webb, "Power requirements of swimming: Do new methods resolve old questions?," Integr. Comp. Biol. **42**, 1018 (2002).

[37]E. D. Tytell and G. V. Lauder, "The hydrodynamics of eel swimming: I. Wake structure," J. Exp. Biol. **207**, 1825 (2004).

[38]I. Borazjani and F. Sotiropoulos, "Numerical investigation of the hydrodynamics of anguilliform swimming in the transitional and inertial flow regimes," J. Exp. Biol. **212**, 576 (2009).

[39]D. B. Quinn, K. W. Moored, P. A. Dewey, and A. J. Smits, "Unsteady propulsion near a solid boundary," J. Fluid Mech. **742**, 152 (2014).

[40]D. B. Quinn, G. V. Lauder, and A. J. Smits, "Flexible propulsors in ground effect," Bioinspiration Biomimetics **9**, 036008 (2014).

[41]P. A. Dewey, A. Carriou, and A. J. Smits, "On the relationship between efficiency and wake structure of a batoid-inspired oscillating fin," J. Fluid Mech. **691**, 245 (2011).